Analysis of light penetration depth in apple tissues by depth- resolved spatial-frequency domain imaging

Tongtong Zhou
Zhejiang A & F University
Dong Hu (20180047@zafu.edu.cn)
Zhejiang A & F University
Dekai Qiu
Zhejiang A & F University
Shengqi Yu
Zhejiang A & F University
Yuping Huang
Nanjing Forestry University
Zhizhong Sun
Zhejiang A & F University
Xiaolin Sun
Zhejiang A & F University
Guoquan Zhou
Zhejiang A & F University
Tong Sun
Zhejiang A & F University
Hehuan Peng
Zhejiang A & F University

Research Article

Keywords: Light penetration depth, apple, spatial-frequency domain imaging, depth-resolved, bruise, scattering

Posted Date: December 12th, 2022

DOI: https://doi.org/10.21203/rs.3.rs-2349216/v1

Additional Declarations: No competing interests reported.

Analysis of light penetration depth in apple tissues by depth-resolved spatial-frequency domain imaging

Tongtong Zhou[1], Dong Hu[1,*], Dekai Qiu[1], Shengqi Yu[1], Yuping Huang[2], Zhizhong Sun[3], Xiaolin Sun[1], Guoquan Zhou[1], Tong Sun[1], Hehuan Peng[1,*]

[1] *College of Optical Mechanical and Electrical Engineering, Zhejiang A&F University, Hangzhou 311300, Zhejiang, China;*

[2] *College of Mechanical and Electronic Engineering, Nanjing Forestry University, Nanjing 210037, China;*

[3] *College of Chemistry and Materials Engineering, Zhejiang A&F University, Hangzhou 311300, Zhejiang, China.*

Corresponding Author:

Dong Hu, Zhejiang A&F University, Email: 20180047@zafu.edu.cn

Hehuan Peng, Zhejiang A&F University, Email: penghh@zafu.edu.cn

Abstract:

Spatial-frequency domain imaging (SFDI) has been developed as an emerging modality for detecting early-stage bruises of fruits, like apples, due to its unique advantage of depth-resolved imaging feature, in comparison with the conventional imaging techniques under uniform or diffuse illumination. This paper presents theoretical and experimental analyses to determine the light penetration depth in apple tissues under spatially modulated illumination. First, light penetrating capacity of the demodulated direct component and amplitude component images was investigated to prove the performance of the constructed SFDI system. Simulation and practical experiments were then carried out to explore the maximum light penetration depths in 'Golden Delicious' apples, in terms of two critical parameters, i.e., image contrast, and ratio of peak-to-valley intensity. Finally, apple experiment for early-stage bruise detection using the estimated reduced scattering coefficient mapping was conducted to validate the results of light penetration depths. The results showed that the simulations produced comparable or a little larger light penetration depth in apple tissues (~2.2 mm) than the practical experiment (~1.8 mm, or ~2.3 mm). Apple peel further decreased the light penetration depth due to the high absorption properties of pigment contents. The apple bruise, located beneath the surface peel with the depth of about 0-1.2 mm, could be effectively detected by the SFDI technique. This study, to our knowledge, made the first effort to investigate the light penetration depth in apple tissues by SFDI, which would provide useful information for enhanced detection of early-stage apple bruising by selecting appropriate spatial frequency.

Keywords: Light penetration depth; apple; spatial-frequency domain imaging; depth-resolved; bruise; scattering.

1. Introduction

Optical sensing techniques, such as near-infrared spectroscopy and hyperspectral imaging, have been extensively researched and increasingly utilized for detecting multiple defects of agro-food products (Askoura et al. 2019, Luo et al. 2022, Yin et al. 2022). The past decade has witnessed the development of spatial-frequency domain imaging (SFDI) for detecting various surface and subsurface defects of fruits (Lu and Lu 2020, Luo et al. 2021, Sun et al. 2022, Fu and Wang 2021). As one of the typical defect type, surface bruise in apples often occurs during harvest, transportation, storage and sorting process. Slight early-stage bruise is invisible to our naked eyes and is challenging to be recognized by traditional imaging techniques under uniform or diffuse illumination, which are more sensitive to the obvious surface properties. Thanks to frequency-dependent light attenuation within tissues, as depicted in Fig. 1, SFDI enables acquiring depth-resolved information regarding tissue constituents and structure. Based on this remarkable feature, SFDI is proven to be capable of detecting the early-stage bruises of apples beneath the peels (Sun et al. 2022). As opposed to the traditional uniform light imaging techniques, like machine vision and hyperspectral imaging, spatially modulated light in a sinusoidal waveform is used in SFDI to acquire pattern images from samples. Through image demodulation and inverse estimation processing, SFDI produces 2-D optical property mappings in a pixel-by-pixel fashion, i.e., absorption coefficient (μ_a) mapping and reduced scattering coefficient (μ'_s) mapping. The differences of optical properties between non-bruised apple tissues and bruised ones can be directly used for early-stage bruise detection. It is well known that there are quite a lot of optical property measuring methods, e.g., time-resolved, spatially-resolved, and integrating sphere, which have been employed for measuring optical properties of diverse agro-food products (Zhang et al. 2019, Liu et al. 2020, Sun et al. 2020, Hu et al. 2020). However, they are generally limited to point measurement and cannot attain depth-resolved information, resulting in

great challenges in the nondestructive detection of early-stage bruise of apples. In the technique of SFDI under the spatially modulated illumination, high-frequency light is more sensitive to the shallower tissue, while low-frequency component has much larger light penetration depth (~mm) (Lu et al. 2016, Lu et al. 2016), which provides a theoretical basis for detecting early-stage bruises of apples.

Knowledge of light penetration depth sampled by SFDI is of high significance for clinical and preclinical applications in the field of biomedicine (Zhao et al. 2020, Pilvar et al. 2022, Lee et al. 2019). For instance, the thickness of burned skin dictates the treatment protocol, highlighting the importance of understanding the detection depth in skin tissue (Nguyen et al. 2013). SFDI has also been explored in deep-tissue applications, where it is essential to understand the penetration of collected photons in order to evaluate the maximum depth of measurable tumor contrast (Robbins et al. 2017). Similar with that in the field of agricultural and food engineering, knowledge of light penetration depth is critical for enhancing detection performance of early-stage bruise in apples by SFDI. Despite great progress being made for bruise detection of apples, there still is a lack of quantifying light penetration depth in apple tissue. As mentioned above, SFDI has remarkable advantage in subsurface (early-stage) bruise detection of apples, but the light penetration depth is reported to be limited in mm, implying that some internal bruises located in the region of deep tissue cannot be detected. It is thus desirable and also necessary to quantify light penetration depths under varying-frequency spatially modulated illumination, so as to better explore the potential of SFDI for early-stage bruise detection of apples in different depths, as well as to assess the severity of apple bruising. Up to now, the maximum detection depth in apple tissue using SFDI is uncertain and there are few researches focusing on studying light penetration depth. Lu and Lu (2019) reported that the maximum light penetration depth was confirmed to be no more than 3 sheets of paper (or less than 400 μm). Their study investigated the light penetration depth from the aspect of

demodulated images, which is different from our research in optical property estimation through inverse computation. The estimated optical property mappings could provide quantitative information in bruise detection (specific values of optical properties for non-bruised and bruised tissues), and thus being worth further exploring the light penetration depth.

Therefore, in this study, a set of well-designed experiments from theoretical simulation to practical implementation was performed to quantify the light penetration depth (especially for the maximum value) in apple tissue under spatially modulated illumination. The objectives were to: (1) explore the light penetrating capacity of demodulated direct component (DC) and amplitude component (AC) images to prove our SFDI system performance; (2) conduct the simulation and practical experiments to investigate the light penetration depths in 'Golden Cream Delicious' apples with and without peels; (3) validate the conclusion of the maximum light penetration depth in apple tissues by evaluating the performance of bruise detection.

2. Theoretical formulation for SFDI

2.1. Image formation and image processing

In SFDI, image formation involves two steps: (1) the incident light interacts with the sample through absorption and multiple scattering, and (2) the light reemitted from the sample travels through a series of optical devices (e.g., lens, camera) of the imaging system, and eventually forms a digital image. As a general rule, SFDI is regarded as a linear, space-invariant technique which applies transfer function theory to an optical imaging system (Goodman 1996). There are several factors negatively affecting the resolution and contrast of resulting images during image formation and process, such as convolution operation and environmental noise. Mathematical method is used to analyze the image acquired by SFDI,

which is generally composed of two parts. The first part is DC , i.e., I_{DC} with the Fourier spectra centered at the origin; the other part is AC termed as I_{AC}, which is composed of oscillatory or harmonic component, with the Fourier spectra shifted by positive or negative frequency (f_x or $-f_x$) (Gustafsson 2005).

The process of optical property estimation from the remitted image in the SFDI can be roughly divided into two steps: acquisition of diffuse reflectance image through demodulation and estimation of optical property mapping through inverse computation. Due to the characters of high-accuracy and easy-to-implementation, phase shifting techniques are widely used for demodulation from sinusoidal fringe patterns. Three-phase demodulation (TPD) is a commonly used and effective method that uses three images with the phase offsets of $-2\pi/3$, 0 and $2\pi/3$. Under the illumination of three phase-shifted sinusoidal patterns, the corresponding intensity images, i.e., $I_1(x,y)$, $I_2(x,y)$ and $I_3(x,y)$, can be expressed as follows (A et al. 1997):

$$I_1(x,y) = I_{DC} + I_{AC}\cos(2\pi f_x x - 2\pi/3) \quad (1)$$

$$I_2(x,y) = I_{DC} + I_{AC}\cos(2\pi f_x x) \quad (2)$$

$$I_3(x,y) = I_{DC} + I_{AC}\cos(2\pi f_x x + 2\pi/3) \quad (3)$$

where (x,y) represents the spatial coordinates, f_x is the spatial frequency along the *x*-axis direction, I_{DC} and I_{AC} are the direct and amplitude components, respectively. For the purpose of simplicity, we will drop off the coordinate notation. From Eqs. (1) - (3), the DC and AC images can be obtained by the following equations (Lu et al. 2016):

$$I_{DC} = \frac{1}{3}(I_1 + I_2 + I_3) \quad (4)$$

$$I_{AC} = \frac{\sqrt{2}}{3}\sqrt{(I_1 - I_2)^2 + (I_1 - I_3)^2 + (I_2 - I_3)^2} \quad (5)$$

2.2. Image contrast

Light penetration features are of primary concern for the demodulated images, which are also critical for fruit bruise detection. To our knowledge, it is challenging to assess the light penetration capability, because it is largely dependent on tissue physicochemical properties and illumination conditions. For the bruised apples illuminated under spatially modulated illumination with varying frequencies, light penetration capability could essentially determine thickness of the tissue that light passes through. In this study, we introduce image contrast and the ratio of peak to valley's intensity (PVR) to evaluate the light penetration capability, which would be introduced in Section 3.2. Examination of the composition of photons backscattered from a turbid medium will provide qualitative insights into the relationship between light penetration depth and image contrast. The ballistic photons experience one or more backward and forward scattering events before exiting from the tissue. Due to the shortest travelling path, they suffer from minimal scattering and thus can deliver image information with superior resolution and contrast. However, the information generated by ballistic photons is more about the superficial layer of the medium in one mean free path (MFP) (Ntziachristos and Vasilis 2010), around 100 μm for fruit tissue like apple (assuming the value of μ'_s is equal to or larger than 1.00 mm^{-1}). The weakly scattered photons provide information on deeper, sub-surface tissues, and they are still capable of forming well-resolved images due to limited scattering events. In summary, the tradeoff should be carefully considered between the light penetration depth and image contrast, while selecting spatial frequency in SFDI (Ntziachristos and Vasilis 2010, Gigan 2017).

The I_{DC}, which contains a larger contribution of diffusive photons, probes a deeper region of sample tissues than I_{AC}, while I_{AC} contains more ballistic and weakly-scattered photons, resulting in better image contrast (Lu et al. 2016). High-frequency illumination is more likely to enhance image contrast.

Presented in the following sections are well-designed experiments to quantitatively determine the relationship between image contrast and depth-resolved imaging feature of SFDI.

2.3. Light penetration

In diffuse optics, the light penetration depth δ in biological tissues can be attained from the response to an infinitely narrow photon beam normally incident on a semi-infinite medium. For the case that photon's propagation depth z is larger than the light penetration depth, internal fluence distribution predicted from diffusion theory should be (Wilson and Jacques 1990):

$$\emptyset(z) = \emptyset_0 \, k \exp(-z/\delta) \tag{6}$$

where k is a scalar that depends on the amount of backscattered reflectance, $\emptyset_0$ is the incident irradiance, $\emptyset(z)$ represents a function of photon fluence. The light penetration depth is defined as (Wang and Jacques 1992):

$$\delta = \frac{1}{\sqrt{3\mu_a(\mu_a+\mu_s(1-g))}} = \frac{1}{\mu_{eff}} \tag{7}$$

where μ_a is the absorption coefficient, μ_s is the scattering coefficient, g is anisotropy factor, and μ_{eff} is the effective attenuation coefficient.

According to this, light penetration depth is estimated to be 1.50-6.00 mm for apple tissues with typical μ_a and μ_s coefficients of 0.01-0.05 mm^{-1} and 9.00-28.00 mm^{-1}, respectively. However, the estimated depth does not always stand for the actually detectable depth for a general imaging system under spatially-extended wide-field or broad-beam illumination. The fluence rate and reflectance properties of spatially modulated photon density plane waves in the SFDI are described in the study of Cuccia et al. , in which the effective penetration depth δ'_{eff} is concisely defined as:

$$\mu'_{eff} = (\mu_{eff}^2 + k_x^2 + k_y^2)^{1/2} = \frac{1}{\delta'_{eff}} \tag{8}$$

where μ'_{eff} is a scalar attenuation coefficient, k_x and k_y are variable coefficients related to spatial frequencies f_x and f_y ($k_x=2\pi f_x$, $k_y=2\pi f_y$), δ'_{eff} is the effective penetration depth, which is inversely proportional to spatial frequency. The above mathematical formula just provides a simple conceptual framework to understand the transmission of modulated scalar photon in a turbid medium. In practice, the detected signal is mostly due to the photons backscattered close to the illumination source, which corresponds to a far more superficial depth of tissue interrogation than that derived from diffuse light attenuation (Bigio and Fantini 2016). This is equivalent to calculate the relative probability that a photon will visit a certain location in tissue before its detection. In the reflectance measurement geometry with spatially modulated illumination, the reemitted light intensity decays by many orders of magnitude within millimeters. Therefore, using the formula to calculate the light penetration depth directly exists some unreasonable aspects. In this study, well-designed experiments were conducted, coupled with two evaluation parameters (image contrast and PVR), to explore the light penetration depth in apple tissues using SFDI.

3. Materials and methods

3.1. SFDI system

An in-house assembled SFDI system, as illustrated in Fig. 2, mainly consisted of a 150-W DC-regulated halogen fiber optic light source (Fiber-Lite DC950, Dolan-Jenner, Boxborough, USA), a light-guide fiber (MSG4-2200S, MORITEX Corporation, Saitama, Japan), a 8-bit camera (MER-131-210U3M NIR, Daheng imaging vision Corporation, Shanghai, China) coupled with a C-mount zoom lens (HN-0816-5M-C2/3X, Daheng imaging vision Corporation, Shanghai, China) for vertically shinning over a field of view (FOV, 11.5×11.5 cm^2), a filter wheel (BOCIC Co., LTD, China) comprising

six bandpass filters (550, 600, 630, 675, 710 and 730 nm), a micro controller unit (MCU) (STM32F103ZET6, Opendv, Guangzhou, China), a three-axis manual displacement platform (THZ210, Runjia Pneumatic, Shenzhen, China) for holding samples, and an optical projector (DL*i*6500 1080p Optics Bundles, TI, Austin, Tex., USA) for generating sinusoidal patterns. The projector was slightly angled at 12 degrees relative to the vertical axis to mitigate the image distortion. The MCU could take control of the projector for synchronous pattern projection and image acquisition with the camera. A pair of cross linear polarizers was mounted in front of the lens of the projector and camera to suppress specular reflectance from samples. The aforementioned components were mounted on an optical platform (SPL-R-0910, SPL-Tech, Hangzhou, China), and enclosed in a dark chamber for reducing the influence of external stray light.

3.2. Experiments

3.2.1. Experiment 1: penetrating capacity of DC and AC images

The first experiment was to verify the light penetrating capacity of DC and AC images and thus proving our SFDI system performance. The experiment was conducted using a highly scattering nylon slab, which was drilled with five cylindrical holes running parallel with the surface. As shown in Fig. 3, the five holes with the diameter of 4 mm or 8 mm were set up at the depths of 1 mm, 11 mm, 6 mm, 4 mm, and 2 mm, from left to right. All the holes were filled with 100-times diluted India ink as absorbers for absorption property comparison with the bull material, and then sealed with adhesive black tape. A sequence of sinusoidal patterns, covering 18 frequencies [0.01:0.01:0.15, 0.20, 0.25, 0.30] mm^{-1}, were generated in Matlab R2020a (The Mathworks, Inc., Natick, MA, USA) for sample illumination. Three phase-shifted pattern images were acquired at each spatial frequency with the phase offsets of $-2\pi/3$,

208 0, $2\pi/3$, respectively. A standard whiteboard with the calibrated reflectance rate of 99% was imaged
209 first under planar illumination to correct the non-uniformity of the source illumination (Sun et al. 2021).
210 Image demodulation was then used to generate the DC and AC images, according to Eqs. (4) and (5).

211 3.2.2. Experiment 2: investigating light penetration depth

212 The second experiment was to quantify the light penetration depth in apple tissue under sinusoidal
213 illumination. 'Golden Cream Delicious' apples, which are free of visual blemishes or defects and grown
214 in Shandong, China, were purchased from a fruit market. Both simulation and practical experiments were
215 carried out. In the first, the simulation methodology proposed by Hayakawa et al. (2019) was adopted to
216 roughly determine the optical sampling depth in apple tissues. In this method, Monte Carlo (MC), which
217 has been widely applied to simulate light propagation in single- and multiple-layered biological tissues,
218 was employed for simulation experiment (Zhang et al. 2019, Wang and Jacques 1992, Hu et al. 2020).
219 Optical property parameters (μ_a, μ'_s) of apple tissues at the six wavelengths were measured by our
220 integrating sphere system (Sun et al. 2022), which were taken as the inputs in the simulation.
221 For the practical experiment for validating the results of the simulations, there are two types of
222 samples, apple slice and a USAF 1951 target. A slicer was used to produce apple slices with different
223 thicknesses with peel [0.9, 1.0-1.1, 1.3, 1.5-1.6, 1.6-1.7, 1.8, 2.1-2.2, 2.4-2.5, 2.6, .3.0, 3.4, 3.8, 4.0] mm
224 and without peel [0.8, 1.0, 1.2-1.3, 1.5, 1.6, 1.8, 2.0, 2.3, 2.5-2.6, 2.7-2.8, 3.0, 3.2, 3.6, 4.0] mm. These
225 varying-thickness apple slices were used to cover the USFA-1951 target, which was made of highly
226 scattering fiber material, and their combination was imaged by the SFDI system, illuminated with a
227 sequence of frequencies of 0.05, 0.10, 0.15, 0.20, 0.25, 0.30 mm^{-1}. It is apparent that the light has
228 completely penetrated though the apple slice while the black horizontal bars of the USFA-1951 are

recognized, as shown in the region of interest (ROI) in Fig. 4. Two parameters in the ROI, i.e., image contrast and PVR, as mentioned above, were calculated to resolve the image details. Image contrast was evaluated based on the Michelson contrast metric (C_M) (Makous 2002) :

$$C_M = (I_{max} - I_{min})/(I_{max} + I_{min}) \quad (6)$$

where I_{max} and I_{min} denote the maximum and minimum intensities of the image in ROI, respectively. Another evaluating parameter PVR, defined as the ratio of peak and valley's intensity(Wang et al. 2012), was also determined from the captured images:

$$PVR = I_{peak}/I_{valley} \quad (7)$$

where I_{peak} and I_{valley} denote the intensities of the peak and valley in the ROI, respectively.

3.2.3. Experiment 3: detecting early bruises in apples

The third experiment was to test and verify the results of light penetration depths in apple tissues achieved from experiment 2. Impact tests were conducted to induce bruises in the apples with a wooden ball attached to one end. The wooden ball (6 cm in diameter, and 105 g in weight) fell freely from the rest position at a certain height to impact the apple at its equatorial area. The peel on the surface of bruised tissue was cut off to eliminate its effect on detection performance. The used frequencies were the same as experiment 2. As shown in Fig. 5, apple slices with and without peels in different thicknesses were used to cover the bruised tissues. Image demodulation and inverse parameter estimation were carried out to obtain the optical property (μ_a and μ'_s) mappings of the apples covered with slices. It is supposed that if the bruised tissue could be recognized in mappings, the light can penetrate through the apple slice, and the light penetration depth under this illumination should be equal to or larger than the thickness of the apple slice.

4. Results and discussion

4.1. Penetrating capacity of DC and AC images

Fig. 6 shows the demodulated DC and AC images of the nylon sample. The filled India ink made the hidden holes relatively dark because of its strong light absorbing capacity. In the DC image (equivalent to uniform illumination), the first hole was easily recognized but with invisibility on the top of the liquid column caused by an unwanted air bubble. The second hole was almost invisible because it was too deep (11 mm) from the tissue surface. For the three hidden holes on the right, the black liquid column became visually fuzzier along with larger distance from the surface. The AC image at the frequency of 0.01 mm^{-1} showed similar details with the DC image. As the frequency increased from 0.02 to 0.12 mm^{-1}, the color of leftmost column became more and more light, and the other columns revealed a reduction on the image invisibility. It was noticed that as the frequency increased, the surface texture of the nylon sample was revealed to a certain degree, with the images becoming less smooth. These observations implied that higher-frequency illumination brought about less light interrogation with deep tissues, resulting in shallower light penetration depth. Similar finding was also reported in the previous study (Lu et al. 2016). When the frequency reached 0.12 mm^{-1}, all the holes became blurry due to insufficient light interrogation. Given all of that, the DC (0 mm^{-1}) image had more light interrogation with deep tissues, while the AC images showed varying light penetration depths and image resolutions with different frequencies. It is suggested that low-frequency component could penetrate deeper into the tissues than the high-frequency part, which is called depth-resolved characteristic of SFDI in this study.

4.2. Investigating light penetration depth

Table 1 showed the measured values of optical property parameters (μ_a, μ'_s) of apple slice without

271 peel using integrating sphere technique. By inputting the optical property values manually into the
272 developed program, light penetration depth for the apple tissue could be simulated by consulting a scaled
273 lookup table derived from MC simulations to the radiative transport equation in the spatial-frequency
274 domain. Fig. 7 displays the simulated results for the apple tissue at six wavelengths (550, 600, 630, 675,
275 710 and 730 nm), in which median sampling depth with [25-75] % fraction of the total measured diffuse
276 reflectance was recognized as critical metrics for light penetration depth (Hayakawa et al. 2019). It was
277 observed that light penetration depths increased slowly with the wavelengths. At 550 nm, median
278 sampling depth with [25-75] % was slightly smaller than that of the other five wavelengths, which was
279 approximately in the range of 0.6-2.2 mm. It demonstrated that the 25-75% measured reflectance had the
280 opportunity to interact with the tissue in the depth of 0.6-2.2 mm. Similarly, Lammertyn et al. (2000)
281 reported that the maximum light penetration depth in Jonagold apples at 692 nm was about 2 mm, which
282 agreed well with the finding in this study. Hence, it was concluded that the light penetration depths in
283 apple tissues were close to each other at the six wavelengths, with the values of no more than 2.2 mm.
284 Fig. 8(a) shows the contrast variation with frequencies for the DC and AC images of the USAF-
285 1951 target covered with apple slice at 630 nm. For both the slices with and without peel, DC images
286 performed almost a constant value of image contrast since they were independent of spatial frequency,
287 while AC images showed much higher contrast values, which rose steadily with the spatial frequency.
288 These findings indicated that AC images, which are unique to SFDI, enhanced image contrast compared
289 to DC images, demonstrating that SFDI is superior to conventional uniform light imaging techniques in
290 image contrast. Fig. 8(b) shows the histogram results of image contrast for the DC images of USAF-
291 1951 target covered with apple slices at the wavelengths of 600, 630, 675, and 710 nm. It was noticed
292 that the contrast values decreased with the thickness of apple tissue, as well as the wavelength. A special

293 case occurs from 675 nm to 710 nm, in which there is a small rise of the contrast for some thicknesses.
294 This is because the reflected signal intensity was generally poor in 630-690 nm due to strong absorption
295 of chlorophyll. When removing the influence of peel (right panel in Fig. 8(b)), there was a steady decrease
296 trend for the image contrast with the wavelength, since the pigment had little effect on apple flesh tissue.
297 Fig. 9 shows statistical results of contrast and PVR at 630 nm for the DC images of USAF-1951
298 target covered with different-thickness apple slices. It was observed that the contrast values in the left
299 chart decreased with the thickness of apple slice. There was an approximate linear relation as the slice
300 thickness ranged from 0.9 mm to 2.5 mm. Similar result was found when analyzing the image contrast
301 in the right chart, with a little narrow thickness range of 1.0-2.5 mm. It was noticed that the distribution
302 of image contrast in the left chart (with peel) was more disperse and irregular than that in the right chart.
303 This could be attributed to the influence of pores on the surface tissue of apple peel. On the other hand,
304 PVR showed a gradual decrease trend with the slice thicknesses. The black horizontal bars of the USFA-
305 1951 target were hardly recognized while PVR was reduced to a certain value. In order to determine the
306 light penetration depth in apple tissue, the threshold value of PVR in the slice thickness range of 0.9-2.5
307 mm, in which a linear relationship between the contrast and slice thickness was observed, was tested by
308 large-scale experiments, and finally set as 1.2. From this aspect, the light penetration depths in apple
309 tissues with and without peels were determined as 0-1.8 mm and 0-2.3 mm, respectively. These results
310 were quite similar with those obtained in the simulation experiments (0-2.2 mm). The differences
311 between the simulation and practical experiments could be caused by many factors. For example, the
312 apple optical properties, which were taken as the inputs in the simulations, are prone to measurement
313 errors of integrating sphere system, and thus leading to deviations for the simulation results. In addition,
314 it is challenging to consider all the experiment details completely, such as the minute space between the

315 covered apple slice and USAF-1951 target, and they may cause potential effects on our data analysis and
316 final results.

317 4.3. Validation in detecting early-stage bruise of apple

318 Experiment on early-stage bruise detection of apples was conducted to validate the results of light
319 penetration depth in apple tissues. The apple was peeled first to make the bruised tissue visible, and then
320 it was covered with different-thickness apple slices with or without peels. Spatial-frequency domain
321 images were acquired, followed with image demodulation and inverse estimation for generating optical
322 property mappings. It was supposed that the bruised apple tissue could be detected if the light penetration
323 depth was equal to or larger than the thickness of the covered apple slice. Fig. 10 shows the demodulated
324 images of the bruised apple covered with 0.8 mm-thickness apple slice without peel. The AC images at
325 certain spatial frequencies enhanced the bruised feature compared with the DC image. Strong contrast
326 and surface texture variation were observed with the increased frequency. These findings indicated the
327 enhanced capability of SFDI for detecting early-stage bruise of the apples, in comparison with the
328 imaging techniques under uniform or diffuse illumination. It was believed that inverse parameter
329 estimation for optical property mappings would provide more useful information for qualitative and
330 quantitative analyses of bruising detecting (Sun et al. 2021). Therefore, the absorption and reduced
331 scattering coefficient mappings were produced in our next step. The previous studies reported that
332 bruising changed the optical properties of apples, particularly the reduced scattering coefficient, resulting
333 in the difference between bruised and non-bruised tissues. The bruising detection based on the reduced
334 scattering coefficient mapping was further analyzed to validate the results of light penetration depth in
335 apples.

336 Fig. 11 shows the reduced scattering coefficient mappings of the bruised apple covered with pre-

337 prepared apple slices, with the bruised tissue marked in red circles. It was noticed that the bruised apple
338 tissue without being covered by any slice, as shown in Fig. 11(a), was clearly observed from the reduced
339 scattering coefficient mapping. Fig. 11(b) showed that the bruised apple tissue covered with the 1.2 mm-
340 thickness slice with peel could still be easily recognized, revealing that the spatially modulated light
341 could completely penetrate through the apple slices with peel with the thickness of 0-1.2 mm. The 1.5
342 mm-thickness slice cover without peel (Fig. 11(d)) provided more difficulty for apple bruise detection
343 than the 0.8-thickness slice (Fig. 11(c)), but both of them could still be penetrated by the light. Through
344 data analysis of all the mapping results with different-thickness slices, it was concluded that the apple
345 slice without peel could be completely penetrated with the thickness range of 0-1.5 mm.

346 According to the report of Binzoni et al. (2008), the number of photons that visit a given tissue voxel
347 situated at a depth larger than 2 mm represents less than the 1% of the total number of photons reaching
348 the corresponding detection pixel. They made the conclusion that the light penetration depth was no more
349 than 2 mm, which confirmed our findings. In addition, Lu and Lu (2019) reported that the maximum
350 light penetration depth was no more than 3 sheets of white paper (or less than 400 μm). In our study, the
351 apple slice, instead of white paper, was used as the cover for experiments, which was more scientific and
352 reasonable for investigating the light penetration depth in apples. It should be pointed out that the results
353 of light penetration depth obtained in this study are based on the apple sample, SFDI system configuration,
354 and data processing method. Zhao et al. (2020) reported that shortwave-infrared illumination could
355 penetrate thicker biological tissue than visible light. Hence, the hardware of the SFDI system, including
356 the camera, the light source and wavelength range, as well as the image processing algorithm, could be
357 improved to increase light penetration depth in the future.

5. Conclusions

This paper presents theoretical and experimental analyses of light penetration depth in apple tissues using SFDI technology. The MC simulation coupled with the developed program indicated that the light penetration depth in apples was no more than 2.2 mm. The practical experiment on the USAF-1951 target covered with different-thickness apple slices demonstrated that the maximum light penetration depths were 1.8 mm with peel and 2.3 mm without peel, which were quite similar with the simulation results (0-2.2 mm). Example experiment on early-stage bruise detection was carried out to validate the light penetration depths in apples. The results showed that the bruised apple tissues covered with the slices with the thicknesses of 0-1.5 mm or 0-1.2 mm could be detected, depending on the presence of the apple peel or not. The maximum depth of apple bruise should be about 1.2 mm beneath the surface peel, otherwise the SFDI technique could not achieve accurate detection. In summary, SFDI can serve as a subsurface imaging technique for detecting early-stage bruise of thin-skinned fruits (< 1.2 mm), like apples. Improvement of system hardware and data processing algorithm may provide potential for increasing the light penetration depth. Further work can be directed to explore the full potential of SFDI in bruise detection of other thin-skinned fruits and vegetables, like pears, peaches, cucumbers and potatoes.

CRediT taxonomy:

Conceptualization: [Dong Hu]; Methodology: [Tongtong Zhou]; Data analysis: [Tongtong Zhou]; Formal analysis and investigation: [Dekai Qiu], [Shengqi Yu], [Zhizhong Sun], [Xiaolin Sun]; Data curation: [Dekai Qiu], [Shengqi Yu]; Writing - original draft preparation: [Tongtong Zhou]; Writing - review and editing: [Dong Hu], [Hehuan Peng]; Funding acquisition: [Dong Hu], [Yuping Huang]; Supervision: [Dong Hu], [Yuping Huang], [Guoquan Zhou], [Tong Sun], [Hehuan Peng]

Funding This research was supported by the National Natural Science Foundation of China (32001414, 32101615) and Natural Science Foundation of Zhejiang Province (LQ20C130002).

Declarations

Ethical Approval This article does not contain any studies with human participants or animals performed by any of the authors.

Informed Consent Not applicable in this study.

Conflict of Interest The authors declare that she has no conflict of interest.

Data Availability Statements

The Data underlying this article will be shared on reasonable request to the corresponding author.

Reference

Askoura ML, Vaudelle F, L'Huillier J-P (2019) Use of steady-state imaging setup for assessing the internal optical properties of non-spherical apple samples. Comput Electron Agric 157:181-188. http://doi.org/10.1016/j.compag.2018.12.049.

Luo W, Fan GZ, Tian P, Dong WT, Zhang HL, Zhan BS (2022) Spectrum classification of citrus tissues infected by fungi and multispectral image identification of early rotten oranges. Spectrochim Acta A 279. http://doi.org/10.1016/j.saa.2022.121412.

Yin H, Li B, Liu YD, Zhang F, Su CT, Ou-yang A (2022) Detection of early bruises on loquat using hyperspectral imaging technology coupled with band ratio and improved Otsu method. Spectrochim Acta A 283. http://doi.org/10.1016/j.saa.2022.121775.

Lu YB, Lu RF (2020) Siritool: A Matlab Graphical User Interface for Image Analysis in Structured-Illumination Reflectance Imaging for Fruit Defect Detection. Trans ASABE 63:1037-1047. http://doi.org/10.13031/trans.13612.

Luo YF, Jiang X, Fu XP (2021) Spatial Frequency Domain Imaging System Calibration, Correction and Application for Pear Surface Damage Detection. Foods 10(9):2151. http://doi.org/10.3390/foods10092151.

Sun ZZ, Hu D, Xie LJ, Ying YB (2022) Detection of early stage bruise in apples using optical property mapping. Comput Electron Agric 194. http://doi.org/10.1016/j.compag.2022.106725.

Fu XP, Wang MY (2021) Detection of Early Bruises on Pears Using Fluorescence Hyperspectral Imaging Technique. Food Anal Methods 15:115-123. http://doi.org/10.1007/s12161-021-02092-3.

Zhang MY, Li CY, Yang FZ (2019) Optical properties of blueberry flesh and skin and Monte Carlo multi-layered simulation of light interaction with fruit tissues. Postharvest Biol Technol 150:28-41. http://doi.org/10.1016/j.postharvbio.2018.12.006.

Liu DY, Xie DD, Guo WC (2020) Effect of CPPU on bulk optical properties of kiwifruit during storage in near-infrared range. J Sci Food Agric 100:3111-3119. http://doi.org/10.1002/jsfa.10345.

Sun Y, Lu RF, Pan LQ, Wang XC, Tu K (2020) Assessment of the optical properties of peaches with fungal infection using spatially-resolved diffuse reflectance technique and their relationships with tissue structural and biochemical properties. Food Chem 321:126704. http://doi.org/10.1016/j.foodchem.2020.126704.

Hu D, Lu RF, Ying YB (2020) Spatial-frequency domain imaging coupled with frequency optimization for estimating optical properties of two-layered food and agricultural products. J Food Eng 277. http://doi.org/10.1016/j.jfoodeng.2020.109909.

Lu YZ, Li R, Lu RF (2016) Fast demodulation of pattern images by spiral phase transform in structured-illumination reflectance imaging for detection of bruises in apples. Comput Electron Agric 127:652-658. http://doi.org/10.1016/j.compag.2016.07.012.

Lu YZ, Li R, Lu RF (2016) Structured-illumination reflectance imaging (SIRI) for enhanced detection of fresh bruises in apples. Postharvest Biol Technol 117:89-93. http://doi.org/10.1016/j.postharvbio.2016.02.005.

Zhao YY, Pilvar A, Tank A, Peterson H, Jiang J, Aster JC, Dumas JP, Pierce MC, Roblyer D (2020) Shortwave-infrared meso-patterned imaging enables label-free mapping of tissue water and lipid content. Nat Commun 11:5355. http://doi.org/10.1038/s41467-020-19128-7.

Pilvar A, Plutzky J, Pierce MC, Roblyer D (2022) Shortwave infrared spatial frequency domain imaging for non-invasive measurement of tissue and blood optical properties. J Biomed Opt 27. http://doi.org/10.1117/1.Jbo.27.6.066003.

Lee SY, Zheng C, Brothers R, Buckley EM (2019) Small separation frequency-domain near-infrared spectroscopy for the recovery of tissue optical properties at millimeter depths. Biomed Opt Express 10:5362-5377. http://doi.org/10.1364/boe.10.005362.

Nguyen JQ, Crouzet C, Mai T, Riola K, Uchitel D, Liaw LH, Bernal N, Ponticorvo A, Choi B, Durkin AJ (2013) Spatial frequency domain imaging of burn wounds in a preclinical model of graded burn severity. J Biomed Opt 18:66010. http://doi.org/10.1117/1.JBO.18.6.066010.

Robbins CM, Raghavan G, Antaki JF, Kainerstorfer JM (2017) Feasibility of spatial frequency-domain imaging for monitoring palpable breast lesions. J Biomed Opt 22:1-9. http://doi.org/10.1117/1.JBO.22.12.121605.

Lu YZ, Lu RF (2019) Structured-illumination reflectance imaging for the detection of defects in fruit: Analysis of resolution, contrast and depth-resolving features. Biosys Eng 180:1-15. http://doi.org/10.1016/j.biosystemseng.2019.01.014.

Goodman JW (1996) Introduction to Fourier Optics. Greenwood Village

Gustafsson MGL (2005) Nonlinear structured-illumination microscopy: Wide-field fluorescence imaging with theoretically unlimited resolution. Natl Acad Sci U.S.A 102:13081-13086. http://doi.org/doi:10.1073/pnas.0406877102.

A M, Neil, Juskaitis, Wilson (1997) Method of obtaining optical sectioning by using structured light in a conventional microscope. Opt lett.

Ntziachristos, Vasilis (2010) Going deeper than microscopy: the optical imaging frontier in biology. Nat Methods 7:603-614. http://doi.org/10.1038/NMETH.1483.

Gigan S (2017) Optical microscopy aims deep. 11:16. http://doi.org/10.1038/nphoton.2016.257.

Wilson BC, Jacques SL (1990) Optical reflectance and transmittance of tissues: principles and applications. IJQE 77:2186-2199.

Wang LH, Jacques SL (1992) Monte Carlo modeling of light transport in multi-layered tissues in standard C. Comput Meth Biomech Biomed Eng 47 (1992) 131-146.

Cuccia DJ, Bevilacqua F, Durkin AJ, Ayers FR, Tromberg BJ (2009) Quantitation and mapping of tissue optical properties using modulated imaging. J Biomed Opt 14:1083-3668. http://doi.org/10.1117/1.3088140.

Bigio IJ, Fantini S (2016) Quantitative Biomedical Optics: Theory, Methods, and Applications.

Sun ZZ, Xie LJ, Hu D, Ying YB (2021) An artificial neural network model for accurate and efficient optical property mapping from spatial-frequency domain images. Comput Electron Agric 188. http://doi.org/10.1016/j.compag.2021.106340.

Hayakawa CK, Karrobi K, Pera V, Roblyer D, Venugopalan V (2019) Optical sampling depth in the spatial frequency domain. J Biomed Opt 24(7). http://doi.org/10.1117/1.JBO.24.7.071603.

Hu D, Sun T, Yao LJ, Yang ZD, Wang AC, Ying YB (2020) Monte Carlo: A flexible and accurate technique for modeling light transport in food and agricultural products. Trends Food Sci Technol. 102:280-290. http://doi.org/10.1016/j.tifs.2020.05.006.

Sun XL, Sun ZZ, Zhou TT, Hu D, Sun T, Yang ZD, Zhou GQ (2022) Optical characterization of liquid phantoms in 500–1000 nm using an improved single integrating sphere system. Infrared Phys Technol 127. http://doi.org/10.1016/j.infrared.2022.104386.

Makous P (2002) Spatial frequency, phase, and the contrast of natural images. J Opt Soc Am A 19:1096-1106.

Wang WL, Li CY, Tollner EW, Rains GC, Gitaitis RD (2012) A liquid crystal tunable filter based shortwave infrared spectral imaging system: Calibration and characterization. Comput Electron Agric 80:135-144. http://doi.org/10.1016/j.compag.2011.09.003.

Lammertyn J, Peirs A, Baerdemaeker JD, Nicola B (2000) Light penetration properties of NIR radiation in fruit with respect to non-destructive quality assessment. Postharvest Biol Technol.

Binzoni T, Vogel A, Gandjbakhche AH, Marchesini R (2008) Detection limits of multi-spectral optical imaging under the skin surface. Phys Med Biol 53:617-636. http://doi.org/10.1008/0031-9155/53/3/008.

Tables

Table 1 Optical property parameters (μ_a, μ'_s) of 'Golden Cream Delicious' apple tissues measured by integrating sphere system at six different wavelengths.

Wavelength (nm)	μ_a (mm^{-1})	μ'_s (mm^{-1})
550	0.0302	1.286
600	0.0232	1.273
630	0.0218	1.259
675	0.0224	1.251
710	0.0222	1.256
730	0.0223	1.256

Figure Captions

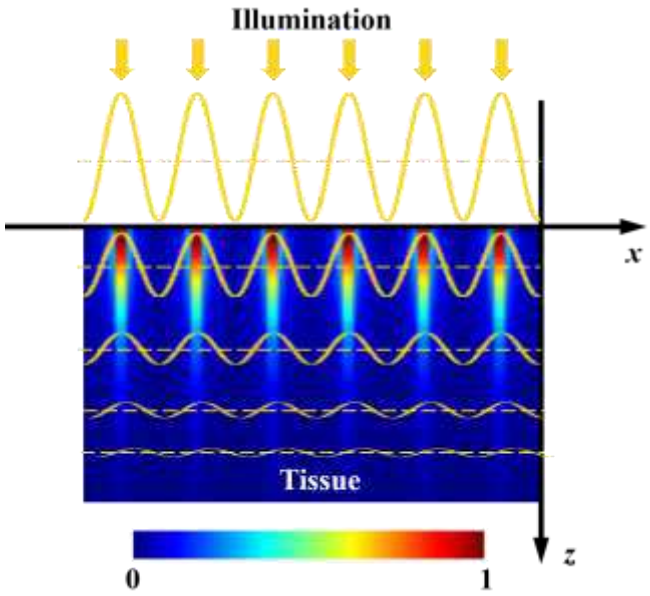

Fig. 1 Schematic of light attenuation within a semi-infinite turbid medium under spatially modulated illumination.

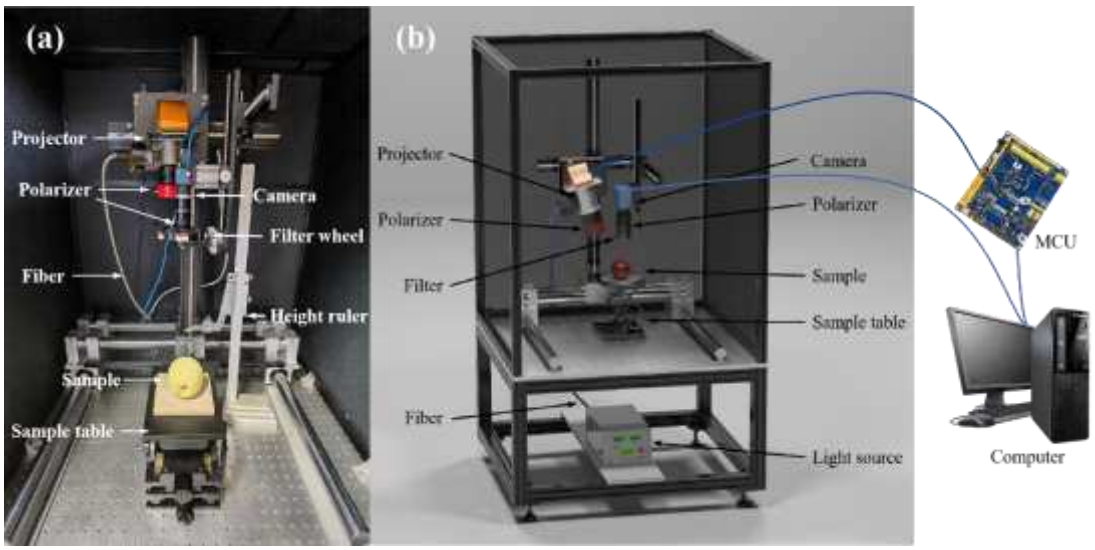

Fig. 2 (a) Physical and (b) schematic maps of spatial-frequency domain imaging system.

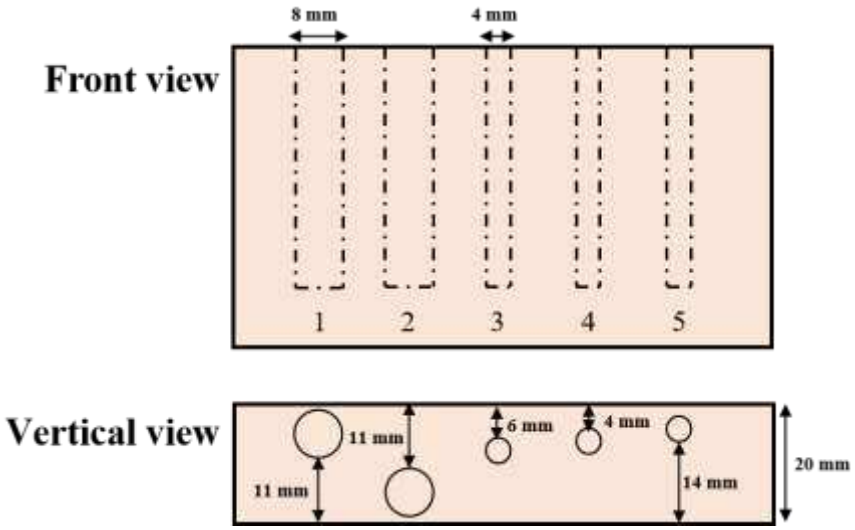

499

500 **Fig. 3** Schematic of relative positions and sizes of holes in the nylon sample filled with absorbing ink solution.

501

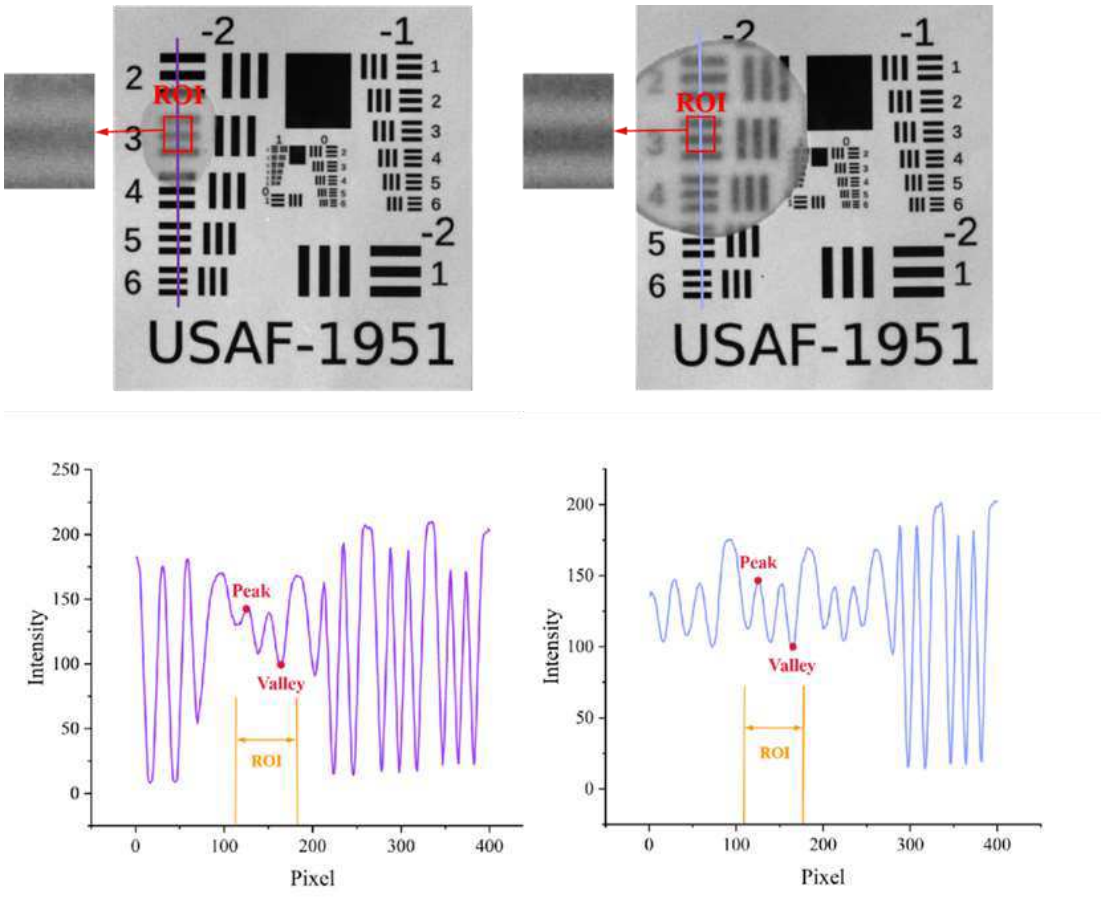

502

503 **Fig. 4** Example images of the USAF-1951 target covered with apple slices with peel (left) and without peel (right)

504 for calculating image contrast (up) and PVR (down) in selected region of interest (ROI).

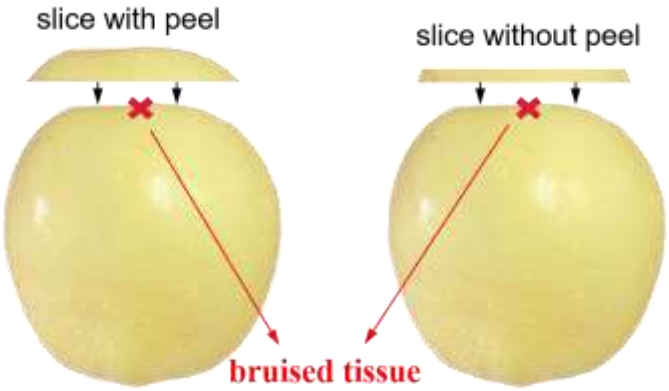

505

506 **Fig. 5** The diagram of peeled bruised apples covering with varying-thickness slices with (left) and without peels

507 (right).

508

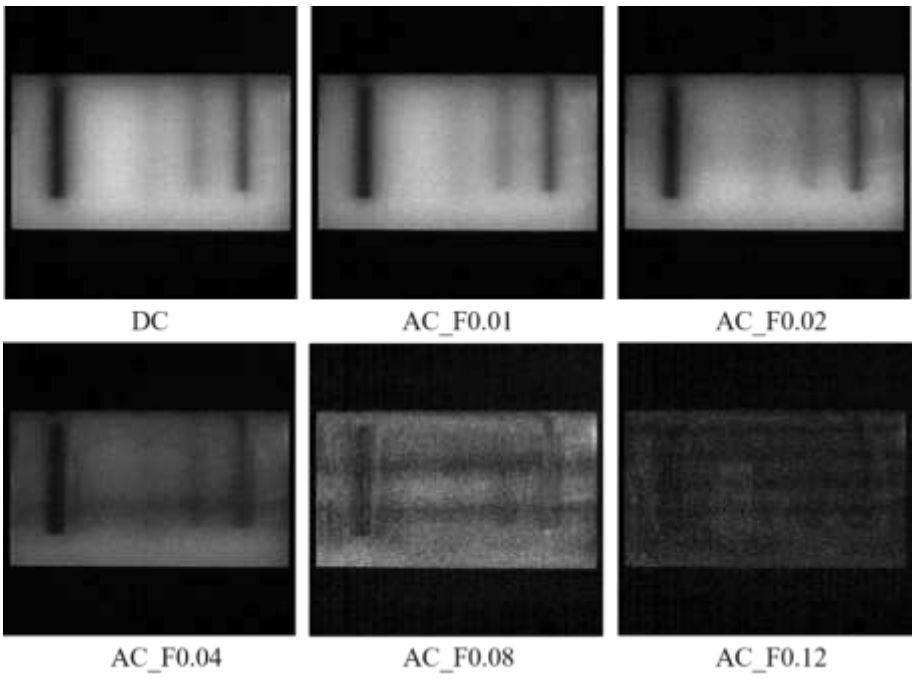

509

510 **Fig. 6** Demodulated DC (direct component) and AC (amplitude component) images of the nylon sample at a

511 sequence of spatial frequencies of 0, 0.01, 0.02, 0.04, 0.08 and 0.12 mm^{-1}, from top left to bottom right.

512

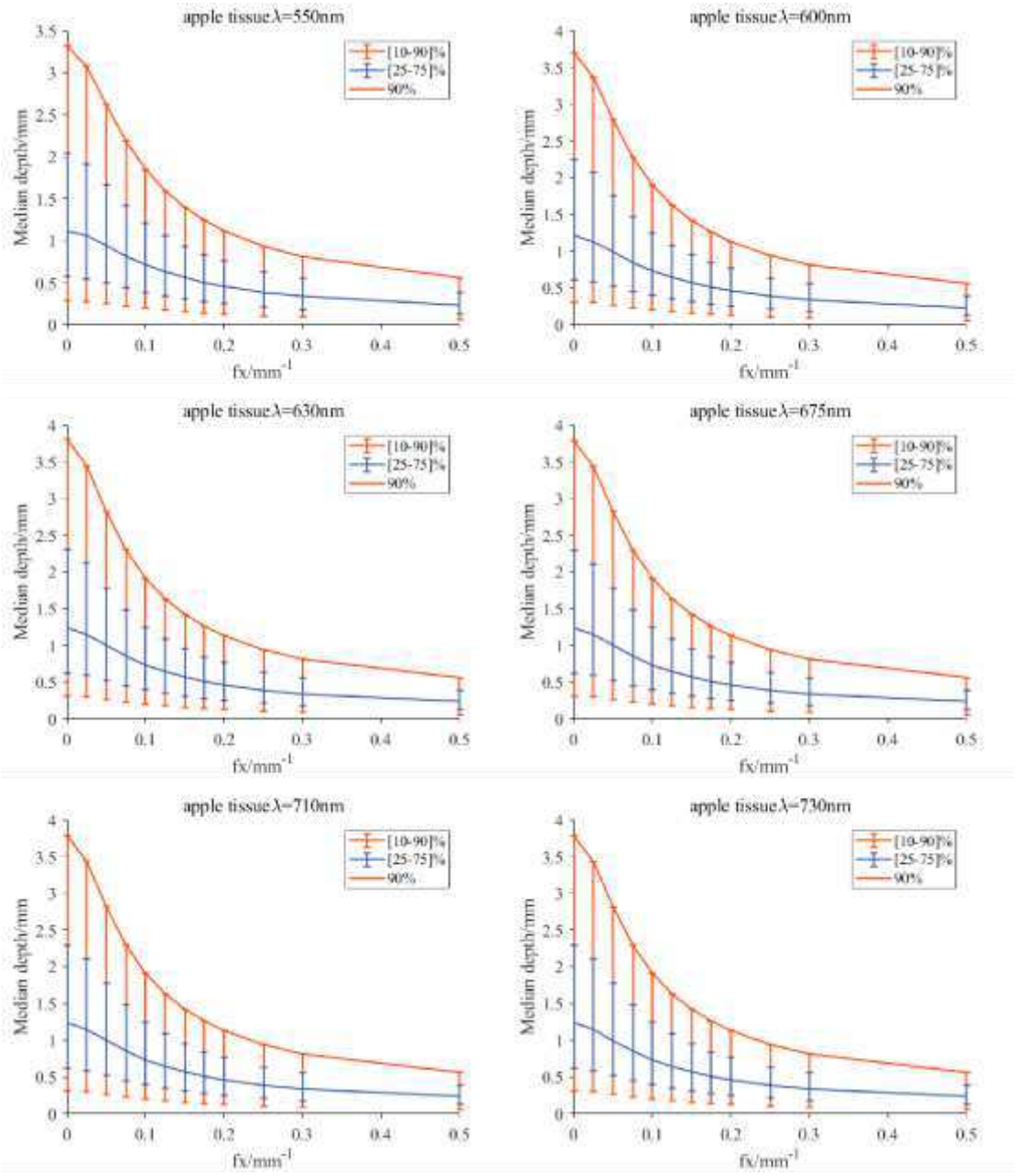

Fig. 7 Simulated median optical detection depth for the apple tissue at six wavelengths, which is estimated using a scaled lookup table derived from MC simulations in the spatial-frequency domain (Hayakawa et al. 2019). The median detection depth is the depth that encloses the photon trajectories responsible for 50% of the detected light, and the vertical-capped lines correspond to detection depths responsible for 25% (lower) and 75% (upper) of the detected light.

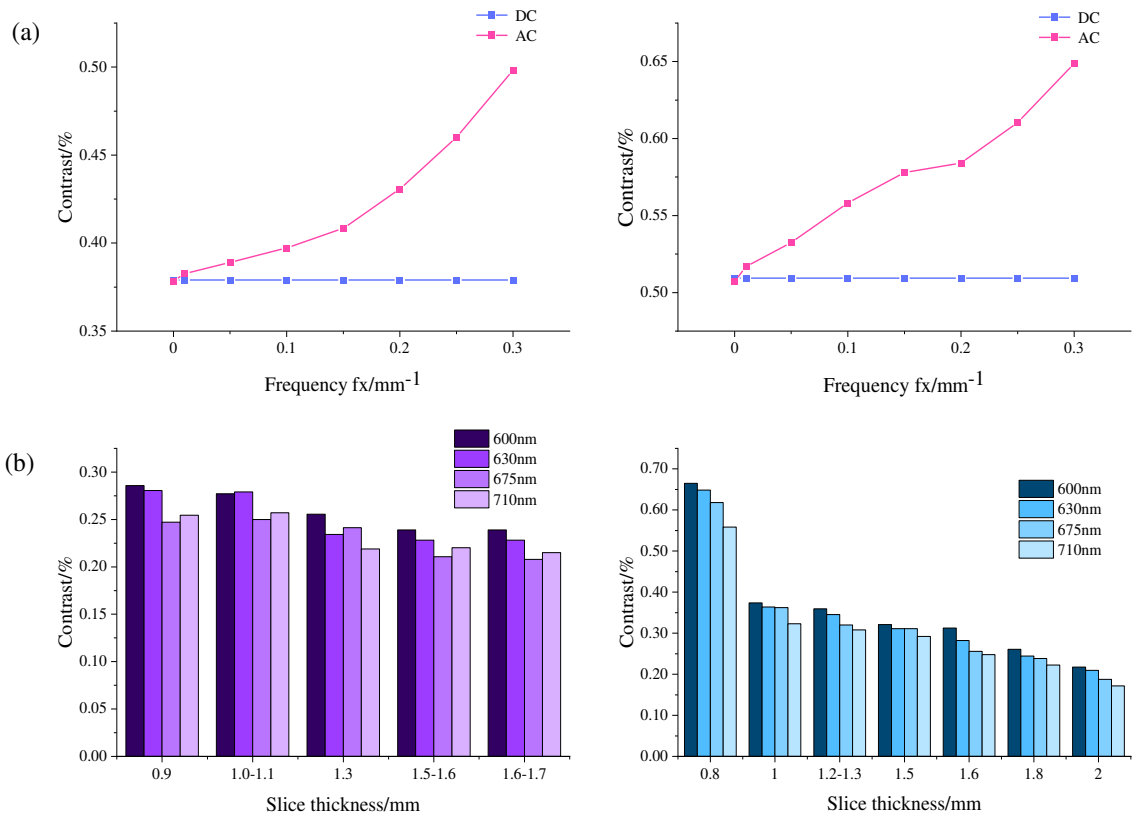

520

521 **Fig. 8** (a) Contrast variation with spatial frequencies for the direct component (DC) and amplitude component (AC)

522 images of USAF-1951 target covered with apple slices with (left) and without peel (right); (b) Histogram of contrast

523 values for the DC images of USAF-1951 target covered with apple slice with (left) and without peel (right) in

524 different thicknesses.

525

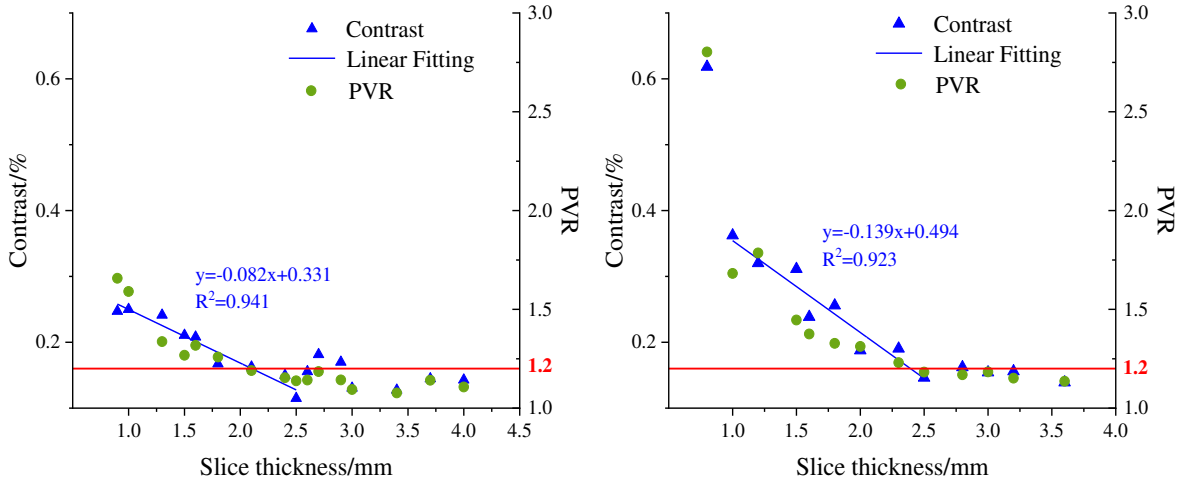

526

527 **Fig. 9** Contrast (left axis) and PVR (right axis) variation at 630 nm for direct component (DC) images of USAF-

528 1951 target covered with different-thickness apple slices (left: with peel; right: without peel).

529

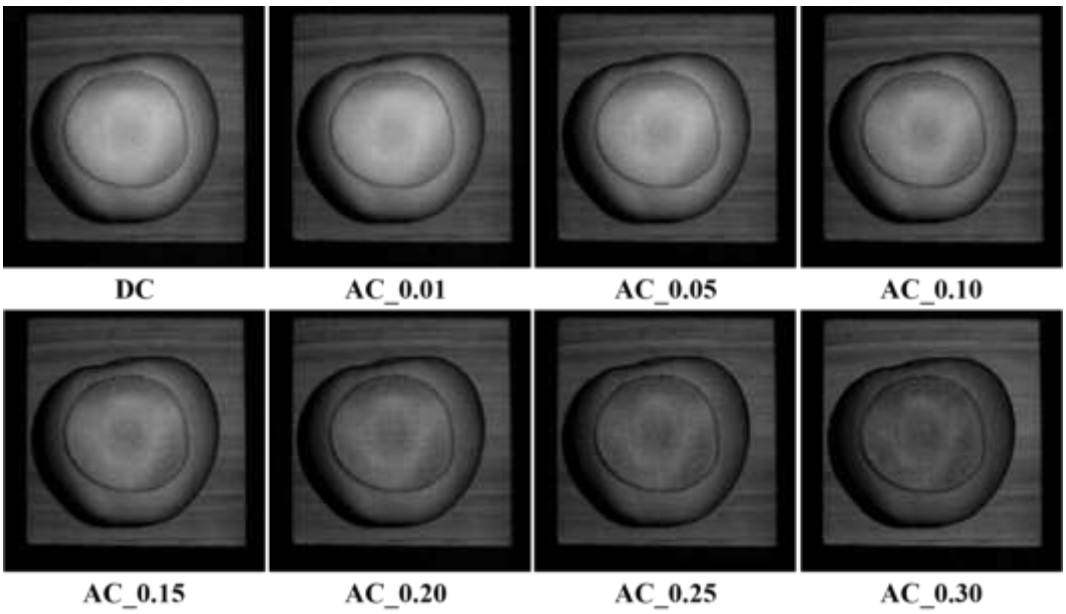

530

531 **Fig. 10** Demodulated images of the bruised apple covered with 0.8 mm-thickness slice without peel at a sequence

532 of spatial frequencies of 0, 0.01, 0.05, 0.10, 0.15, 0.20, 0.25 and 0.30 mm^{-1}, from top left to bottom right.

533

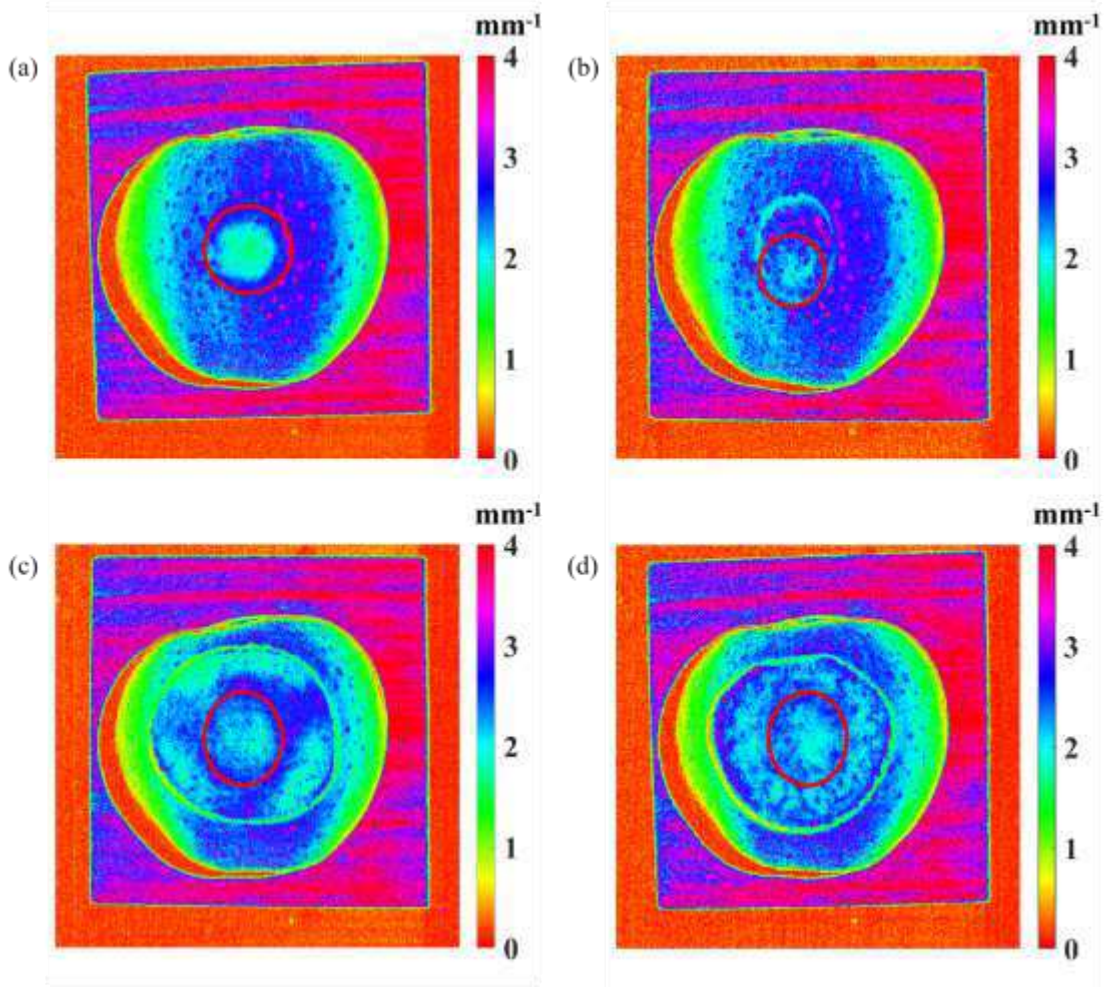

534

535 **Fig. 11** The reduced scattering coefficient mappings of the bruised apple covered without any slice (a), with 1.2 mm-

536 thickness slice with peel (b), and with 0.8 mm-thickness (c) and 1.5 mm-thickness (d) slices without peel.

537